⌘ *Author's Choice*

THE JOURNAL OF BIOLOGICAL CHEMISTRY VOL. 287, NO. 6, pp. 3885–3897, February 3, 2012

AMF-26, a Novel Inhibitor of the Golgi System, Targeting ADP-ribosylation Factor 1 (Arf1) with Potential for Cancer Therapy*[S]

Received for publication, October 25, 2011, and in revised form, December 6, 2011 Published, JBC Papers in Press, December 9, 2011, DOI 10.1074/jbc.M111.316125

Yoshimi Ohashi[‡], Hiroshi Iijima[§], Noriyuki Yamaotsu[§], Kanami Yamazaki[‡], Shigeo Sato[¶], Mutsumi Okamura[‡], Kenji Sugimoto[‖], Shingo Dan[‡], Shuichi Hirono[§], and Takao Yamori[‡1]

From the Division of [‡]Molecular Pharmacology and [¶]Experimental Chemotherapy, Cancer Chemotherapy Center, Japanese Foundation for Cancer Research, Tokyo 135-8550, Japan, the [§]School of Pharmacy, Kitasato University, Tokyo 108-8641, Japan, and the [‖]Laboratory of Applied Molecular Biology, Division of Applied Biochemistry, Graduate School of Agriculture and Biological Sciences, Osaka Prefecture University, Osaka 599-8531, Japan

Background: Golgi is a potential target for cancer treatment, but no inhibitor became an anticancer drug.
Results: Using a unique bioinformatics approach, we identified a novel Golgi inhibitor, AMF-26, targeting Arf1 activation and possessing potent antitumor activity.
Conclusion: AMF-26 is a promising new anticancer drug lead.
Significance: Our data indicate that Arf1 activation is a promising target for cancer treatment.

ADP-ribosylation factor 1 (Arf1) plays a major role in mediating vesicular transport. Brefeldin A (BFA), a known inhibitor of the Arf1-guanine nucleotide exchange factor (GEF) interaction, is highly cytotoxic. Therefore, interaction of Arf1 with ArfGEF is an attractive target for cancer treatment. However, BFA and its derivatives have not progressed beyond the pre-clinical stage of drug development because of their poor bioavailability. Here, we aimed to identify novel inhibitors of the Arf1-ArfGEF interaction that display potent antitumor activity *in vivo* but with a chemical structure distinct from that of BFA. We exploited a panel of 39 cell lines (termed JFCR39) coupled with a drug sensitivity data base and COMPARE algorithm, resulting in the identification of a possible novel Arf1-ArfGEF inhibitor AMF-26, which differed structurally from BFA. By using a pulldown assay with GGA3-conjugated beads, we demonstrated that AMF-26 inhibited Arf1 activation. Subsequently, AMF-26 induced Golgi disruption, apoptosis, and cell growth inhibition. Computer modeling/molecular dynamics (MD) simulation suggested that AMF-26 bound to the contact surface of the Arf1-Sec7 domain where BFA bound. AMF-26 affected membrane traffic, including the *cis*-Golgi and *trans*-Golgi networks, and the endosomal systems. Furthermore, using AMF-26 and its derivatives, we demonstrated that there was a significant correlation between cell growth inhibition and Golgi disruption. In addition, orally administrated AMF-26 (83 mg/kg of body weight; 5 days) induced complete regression of human breast cancer BSY-1 xenografts *in vivo*, suggesting that AMF-26 is a novel anticancer drug candidate that inhibits the Golgi system, targeting Arf1 activation.

Protein-protein interactions (PPIs)[2] play an important role in many biological processes, such as growth, cell survival, and intercellular signal transduction (1, 2). Therefore, inhibitors of specific PPIs can act as novel therapeutic agents including anticancer drugs. Indeed, several small molecule-PPI inhibitors have been developed, such as Nutlin-3 for HDM2-p53 interaction (3), and ABT-737, a Bcl-2 family protein inhibitor (4). Nonetheless, the number of promising PPI inhibitors for cancer treatment remains limited.

In this study, we focused on the activation of ADP-ribosylation factors (Arfs) by its guanine nucleotide exchange factors (GEFs). Arfs are members of the Ras superfamily of small GTPases that play a major role in mediating vesicular transport in the secretory and endocytic pathways (5). The cellular activity of Arfs is stimulated by the Sec7 domain of GEFs that promote the exchange of inactive GDP-bound forms to active GTP-bound forms (6). Arf1, the best characterized Arf, localizes primarily to the Golgi apparatus and regulates both anterograde and retrograde vesicular traffic (7). The first identified small molecule PPI that targets the interaction between Arf-ArfGEF was brefeldin A (BFA, Fig. 1*A*), a lactone isolated from fungi, which inhibits the activation of Arf1 by a subset of its GEFs (8, 9). Treatment of BFA causes rapid but reversible disruption of the Golgi apparatus leading to the vesiculation of the *cis*-Golgi and *trans*-Golgi network (TGN) (10, 11). Furthermore, BFA showed tumor growth inhibition *in vitro* (12) and *in vivo* at an early stage (13). Therefore, inhibitors of Arf1-ArfGEF interaction are valuable tools for studying membrane traffic as well as anticancer drug candidates. However, BFA and its deriv-

* This work was supported by Grants-in-aid for Scientific Research (A) 22240092 from the Japan Society for the Promotion of Science (to T. Y.) and Grant-in-aid for Scientific Research on Priority Areas 11177101 from the Ministry of Education, Culture, Sports, Science and Technology (to T. Y.).
⌘ *Author's Choice*—Final version full access.
[S] This article contains supplemental Tables S1 and S2, Fig. S1, "Experimental Procedures," and Video S1.
[1] To whom correspondence should be addressed. Tel.: 81-3-3520-0111; Fax: 81-3-3570-0484; E-mail: yamori@jfcr.or.jp.

[2] The abbreviations used are: PPI, protein-protein interaction; Arf, ADP-ribosylation factor; BFA, brefeldin A; BIG, brefeldin A-inhibited guanine nucleotide-exchange proteins; CLCa, clathrin light chain a; COP, coat protein complex; ER, endoplasmic reticulum; ERGIC, ER-Golgi intermediate compartment; GBF1, Golgi-specific brefeldin A resistance factor 1; GEF, guanine nucleotide exchange factor; JFCR39, a panel of 39 human cancer cell lines; TGN, *trans*-Golgi network; PARP, poly(ADP-ribose) polymerase; MD, molecular dynamics; HP, hydrophobic.

atives have not progressed beyond the pre-clinical stage of drug development (13, 14).

We previously established a panel of 39 cell lines (termed JFCR39) coupled with our own drug sensitivity data base, which is comparable with that of the NCI60 panel from the National Cancer Institute (NCI) (15–19). Using the COMPARE computer algorithm (details described under "Results"), it is possible to correlate the growth inhibitory patterns of JFCR39 (termed "fingerprints") of a test compound with those of known anticancer drugs and inhibitors (20, 21). Here, we have attempted to identify new Arf1-ArfGEF inhibitors with equivalent functions to BFA but with a different chemical structure, by using COMPARE-guided *in silico* screening instead of structure-based screening.

This approach enabled us to discover a novel small molecule AMF-26 (Fig. 1*B*), an octahydronaphthalene derivative, which disrupts the Golgi system probably by inhibiting the Arf1 activation. AMF-26 shows strong growth inhibition against JFCR39 cell lines *in vitro*. Furthermore, it showed potent antitumor activity against xenografts of the human breast cancer cell line BSY-1 via oral administration.

EXPERIMENTAL PROCEDURES

Chemicals—AMF-26 ((2*E*,4*E*)-5-((1*S*,2*S*,4a*R*,6*R*,7*S*,8*S*,8a*S*)-7-hydroxy-2,6,8-trimethyl-1,2,4a,5,6,7,8,8a-octahydronaphthalen-1-yl)-2-methyl-*N*-(pyridin-3-yl-methyl)penta-2,4-dienamide) and its derivatives were synthesized from AMF-14, a natural product from the genus *Trichoderma*, and kindly provided by the Research Laboratories Kyoto, Nippon Shinyaku Co., Ltd. (Kyoto, Japan). Details of the synthesis methods and the chemical properties of the final product are described under supplemental "Experimental Procedures." BFA and nocodazole were purchased from Sigma, and bafilomycin A1 was purchased from Tocris Bioscience (Bristol, UK). For *in vitro* studies, these compounds were reconstituted to 10 mM in DMSO (Sigma) and stored at −20 °C. For animal experiments, AMF-26 was suspended in 0.05% Cremophor EL (Sigma-Aldrich) in water as a solid dispersion. The antibodies for immunostaining were as follows: monoclonal to anti-GBF1 (clone 25), anti-adaptin γ (clone 88), and anti-adaptin δ (clone 18) were purchased from BD Biosciences (San Jose, CA), anti-ERGIC53 (clone G1/93) was from ALEXIS Biochemicals (Farmingdale, NY), anti-Arf (clone 1D9) and anti-Arf1 (clone EP442Y) were from Abcam (Cambridge, United Kingdom), and anti-α tubulin (clone B-5-1-2) was from Sigma. Rabbit polyclonal to anti-βCOP was from Abcam, and anti-cleaved poly(ADP-ribose) polymerase (PARP) was from Cell Signaling Technology (Boston, MA). Fluorescent probe LysoTracker was purchased from Invitrogen. For Western blotting, horseradish peroxidase-conjugated donkey anti-rabbit or sheep anti-mouse IgG (GE Healthcare) was used as a secondary antibody. For immunofluorescence microscopy, Alexa 488-conjugated goat anti-rabbit or anti-mouse IgG (Molecular Probes, Eugene, OR) was used as a secondary antibody.

Cell Lines—A panel of 39 human cancer cell lines (termed JFCR39, described previously (22)) was used for the *in vitro* experiments. BSY-1 (human breast cancer) cells were also used for *in vivo* studies. MDA-MB-435 (human breast cancer) cells stably expressing GFP-tagged human clathrin light chain a (MDA-MB-435/GFP-CLCa) were prepared as described previously (23). HEK293T (human embryonic kidney) cells were purchased from American Type Culture Collection (Manassas, VA). JFCR39 and MDA-MB-435/GFP-CLCa cells were cultured in RPMI 1640 medium (Wako Pure Chemical Industries) supplemented with 5% fetal bovine serum, penicillin (100 units/ml), and streptomycin (100 μg/ml) in a humidified atmosphere including 5% CO_2 at 37 °C. HEK293T was cultured in DMEM (Wako Pure Chemical Industries) supplemented with 10% heat-inactivated fetal bovine serum and kanamycin, at 37 °C under 5% CO_2. For *in vivo* studies, BSY-1 cells were grown as subcutaneous tumors in nude mice.

Analysis of Cell Growth Inhibition—The inhibition of cell proliferation was assessed by measuring changes in total cellular protein in a culture of each of the JFCR39 cell lines after 48 h of drug treatment by use of a sulforhodamine B assay (24). The 50% growth inhibition (GI_{50}) value was calculated as described previously (18, 19).

COMPARE Analysis—Based on these sets of GI_{50} values, fingerprints are presented in the graphic profiles of relative sensitivity within JFCR39. To analyze the correlation between the fingerprints of drug A and drug B, we exploited the COMPARE computer algorithm as described previously (18, 20, 22). The Pearson correlation coefficient between the fingerprints of drug A and drug B was calculated ($n = 39$).

Live Imaging—MDA-MB-435/GFP-CLCa cells were grown in a 35-mm glass-bottomed dish (Matsunami Glass Ind., Osaka, Japan) for 48 h. Subsequently, the cells were treated with chemicals and imaged on the temperature-controlled stage top incubator (Tokai Hit Co., Shizuoka, Japan) of fluorescent microscopy IX81 (Olympus Corp.) with a ×60 oil, NA 1.35 objective at 37 °C under 5% CO_2. Temperature and CO_2 concentration were maintained with an INUG2A control unit (Tokai Hit Co.). MetaMorph Software (Molecular Devices, Downingtown, PA) was used to control image acquisition and manipulation. For time-lapse observation, images were recorded as described previously by Sakaushi *et al.* (23).

Arf-GTP Pulldown Assay—The pulldown assay to estimate the signals of GTP-bound Arfs was performed as described previously (25, 26). Every pulldown assay was performed with the VHS and GAT domains of human GGA3, cloned, and purified according to a published protocol (25, 26) with modifications as described under supplemental "Experimental Procedures."

We examined the guanine nucleotide exchange activity of endogenous Arfs as follows. BSY-1 cells treated with chemicals for 1 h were scraped into 0.5 ml of cold pulldown buffer containing 50 mM Tris-HCl, pH 7.5, 100 mM NaCl, 2 mM $MgCl_2$, 0.1% SDS, 0.5% sodium deoxycholate, 1% Triton X-100, 10% glycerol, and protease inhibitors mixture (Nacalai Tesque Inc., Kyoto, Japan). The cell lysate was cleared using GSH-Sepharose 4B beads. Then the lysate was gently rotated with the beads containing 50 μg of rGST-GGA3 protein for 30 min at 4 °C. Bound proteins were washed three times with cold wash buffer (50 mM Tris-HCl, pH 7.5, 100 mM NaCl, 2 mM $MgCl_2$, 1% Nonidet P-40, 10% glycerol and protease inhibitors mixture), followed by boiling for 5 min with SDS sample buffer. Proteins in the samples were separated in 10–20% Multi-Gel II mini (Cosmo Bio Co., Tokyo, Japan), followed by electroblotting onto a polyvinylidene difluoride membrane (GE Healthcare).

After immunoblotting analysis using anti-*pan*-Arf and Arf1-specific antibody, immunoreactive bands were identified with the ECL Plus Western blotting detection system (GE Healthcare). Band intensity was determined using the program ImageJ (National Institute of Health).

To confirm the inhibitory efficacy of Arf1 activation, HEK293T/Arf1-HA cells were used to measure exogenous Arf1-GTP. Using the Lipofectamine 2000 reagent (Invitrogen) according to the manufacturer's instructions, HEK293T cells were transfected with the Arf1-HA expression vector, prepared as described under supplemental "Experimental Procedures." For transfection, HEK293T cells were seeded at a density of 3×10^6 cells/10 ml in a 10-cm plate. The transfectants were then incubated for 24 h, and subsequently treated with chemicals for 1 h. The cell lysates were assayed as described above. Because of a difference in molecular weight, the exogenous band of Arf1-HA can be differentiated from the endogenous band of intact Arf1. In HEK293T/Arf1-HA cells, the expression of intact Arf1 was very low. Therefore, the intensity of the band corresponding to Arf1 was apparently weaker than that of the exogenous Arf1-HA.

Conformational Sampling of AMF-26—Conformational analysis of AMF-26 was performed on an Apple Power Mac G5 (PowerPC G5, 2.5 GHz; two central processing units), using the Conformational Analyzer with Molecular Dynamics and Sampling (CAMDAS) 2.1 program (27). Ten molecular dynamic (MD) calculations were simultaneously performed using different initial structures. Each of the MD calculations was carried out for 1 ns with an integral time step of 1 fs. The lengths of the covalent bonds were fixed. The temperature of the system was maintained at 1,200 K to enhance the sampling efficiency. Conformers were sampled every 100 steps, and then each conformer was minimized until the root mean square of the gradients of the potential energy was below 0.001 kcal mol^{-1} $Å^{-1}$. All conformations were clustered with torsion angles of heavy atoms using a threshold of ±30°. The Merck Molecular Force Field 94s was used to evaluate the potential energy surface of the molecule (28, 29). The dielectric constant was 80, but no cut-off distance for non-bonded interactions was used. Because of the low probability of the existence of conformers with higher energies, the conformers within 15 kcal mol^{-1} of the minimum energy of the molecule were adopted for superposition.

Molecular Modeling of the Arf1-AMF-26-Sec7 Domain Complex—To obtain the initial structure of the Arf1-AMF-26-Sec7 domain complex, the sampled conformers of AMF-26 were superposed onto BFA in the X-ray structure of the Arf-BFA-Sec7 domain complex (PDB code 1r8q) (8) using the parallel version of the SUPERPOSE program (30). This superposes two molecules based on the physicochemical properties of the atomic groups, which is useful for estimating the binding conformation of a molecule by distinguishing it from the many conformations that are generated by CAMDAS. The program considers five types of physicochemical property: hydrophobic (HP), aromatic (AR), hydrogen-bond donors (HD), hydrogen-bond acceptors (HA), and hydrogen-bond donors/acceptors (DA). Each type is represented as a sphere with a predefined radius (1.0 or 0.5 Å) and is assigned to a functional group in a molecule (Fig. 4, *A* and *B*). After molecular superposition, the matching spheres were scored using the scoring matrix (supplemental Table S1). One AMF-26 conformation was chosen as the binding conformation based on the scores and the overlapped molecular volumes (Fig. 4*C*). The superposition calculations were performed using 28 nodes of a Dell PowerEdge 1950III (Intel Quad Core Xeon X5460; 3.16 GHz; 56 central processing units in total). The overlapped molecular volumes were calculated by SYBYL 7.3 (Tripos Inc., St. Louis, MO) on an Hewlett Packard work station xw8200 (Intel Xeon; 3.60 GHz; 2 central processing units).

To relieve the steric hindrances, the coordinates of AMF-26 and of the residues within 4 Å from AMF-26 were optimized to reduce the root mean square of the gradients of potential energy below 0.05 kcal mol^{-1} $Å^{-1}$ using SYBYL. The simplex minimization method before the conjugate-gradient minimization procedure was used. The Tripos force field was employed for the molecular energy calculation. The AMBER 4.1 charges (31) were used as the atomic charges for the proteins and the Gasteiger-Hückel charges (32–35) were used as the charges for AMF-26. The cut-off distance for the non-bonded interactions was 8 Å. The distance-dependent dielectric constant of 4r was used. The initial positions of the missing atoms in the crystal structure were generated by the SYBYL.

Molecular Dynamics Simulation for Model Refinement—To refine the model of the Arf1-AMF-26-Sec7 domain complex, AMBER 9 (36) was used for further minimization and MD simulations on 7 nodes of an Appro 1122Hi (AMD Opteron 248; 2.20 GHz; 14 central processing units in total). The ff99 (37) and gaff (38) force fields were used for the proteins and AMF-26, respectively. The partial charges for AMF-26 were derived from the restraint electrostatic potential method (39) using an *ab initio* calculation at the HF/6–31G* level using Gaussian 03 (40). The complex was solvated in a box of 34616 TIP3P (41) water molecules. Six K^+ ions were added to neutralize the system. The system was minimized until the root mean square of the gradients of potential energy was below 0.005 kcal mol^{-1} $Å^{-1}$. The 3.5-ns MD simulation was carried out at constant pressure (1 atm) and temperature (310 K), under periodic boundary conditions, and with particle-mesh Ewald treatment (42) of electrostatics. SHAKE (43) was applied to all bonds involving hydrogen, and a time step of 1 fs was used. An 8-Å cutoff was used for the non-bonded interactions.

Immunofluorescence Microscopy—After being cultured in a 24-well glass bottom plate for 48 h, cells were treated with chemicals for various periods of time (as indicated in the relevant figure). Cells were washed with PBS, fixed with cold 3.8% paraformaldehyde in PBS (Wako Pure Chemical Industries, Osaka, Japan) for 20 min, and then washed and permeabilized with 0.4% Triton X-100 (Sigma) in PBS for 10 min at room temperature. Cells were incubated in blocking buffer containing 1% BSA and 2% normal goat serum (Dako, Glostrup, Denmark) for 30 min before overnight incubation at 4 °C with primary antibodies diluted in blocking buffer. After being washed, cells were incubated for 1 h with secondary antibodies. Cells were then washed, stained with DAPI (Molecular Probes), and mounted with fluorescent

mounting medium (Dako). The immunostained cells were imaged using a fluorescent microscope IX81 (Olympus Corp., Tokyo, Japan) with a ×100 oil, NA 1.40 objective or with a ×40, NA 0.95 objective, and MetaMorph Software (Molecular Devices, Sunnyvale, CA).

Transferrin Recycling Assay—Transferrin recycling was monitored by modification of a previously published assay (44). 6×10^4 cells were incubated in 24-well glass bottom plates for 48 h, and then in serum-free medium for 3 h to deplete endogenous transferrin. After incubation with 20 μg/ml of Alexa Fluor 488-tagged transferrin (Molecular Probes) in PBBS for 1 h, cells were treated with chemicals for 1 h. Cells were then fixed with 3.8% paraformaldehyde in PBS for 20 min at RT, washed with PBS containing 0.1% 1,4-diazabicyclo[2.2.2]octane (DABCO, Sigma), and mounted with fluorescent mounting medium (Dako).

Flow Cytometry—Cells were harvested, washed with ice-cold PBS, and fixed in 70% ethanol. Cells were then washed twice with ice-cold PBS again, treated with RNase A (500 μg/ml; Sigma) at 37 °C for 1 h, and stained with propidium iodide (25 μg/ml; Sigma). The DNA content of the cells was analyzed with a flow cytometer (FACSCalibur, BD Biosciences).

Animal Experiments—Antitumor effect of AMF-26 was tested *in vivo* against human BSY-1 xenografts in mice. Animal care and treatment was performed in accordance with the guidelines of the Animal Use and Care Committee of the Japanese Foundation for Cancer Research, and conformed to the NIH Guide for the Care and Use of Laboratory Animals. Female nude mice with BALB/c genetic backgrounds were purchased from Charles River Japan, Inc. (Yokohama, Japan), maintained under specific pathogen-free conditions, and provided with sterile food and water *ad libitum*. Each nude mouse was subcutaneously inoculated with the generated tumor fragment of size 3 × 3 × 3 mm. When the tumors reached a volume of 100–300 mm^3, animals were randomly divided into control and AMF-26 groups (each group containing five mice) and daily administration of AMF-26 was then started (day 0). We examined the toxic dose of AMF-26 at a single oral administration. The maximum tolerable dose turned out to be 100 mg/kg of body weight. The experimental group of mice was orally administered a given dose of AMF-26 (83 or 100 mg/kg of body weight) on a daily basis from day 0 to 5. The control group of mice was orally administered with 0.05% Cremophor EL (Sigma) instead of AMF-26. Tumor volume of the tumor-bearing mice was measured as described previously (22). The length (L) and width (W) of the subcutaneous tumor mass of live mice were measured using calipers. Tumor weight was calculated as tumor weight = $(L \times W^2)/2$. To assess toxicity, the body weights of the tumor-bearing mice were measured.

Statistical Analysis—Pearson correlation coefficients were calculated for the COMPARE analysis and statistical correlation. The two-sided Mann-Whitney *U* test was used to assess the statistical significance of the antitumor efficacy of AMF-26 in relative tumor growth ratio on days 3, 7, 11, 14, 17, and 21. The number of samples is indicated in the description of each experiment. All statistical tests were two-sided.

RESULTS

Identification of AMF-26 as a Possible Arf1-ArfGEF Inhibitor by COMPARE Analysis—The JFCR39 panel is a powerful tool for the *in silico* screening of compounds with specific pharmacological activities but with different chemical structures. Seed compounds with desirable pharmacological activities can be used to extract candidates with a similar mode of action in the data base by COMPARE analysis. The data base of our cell line panel holds information on 4,000 compounds, including anticancer drugs and known inhibitors of various biological pathways. Employing this protocol, JFCR39 has been successful in identifying several new anticancer agents, such as a new telomerase inhibitor (FJ5002) (45), an inhibitor of topoisomerase I and II (MS-247) (19), and a novel phosphatidylinositol 3-kinase inhibitor (ZSTK474) (22, 46, 47). For instance, the novel PI3K inhibitor ZSTK474 was structurally different from the known PI3K inhibitor LY294002, although their respective fingerprints were similar. We therefore reasoned that COMPARE analysis would be a suitable method for screening structurally diverse compounds to identify those with a similar mode of action to BFA.

When BFA was used as a seed in COMPARE analysis, AMF-26 was identified to be the compound with a highest correlation coefficient ($r = 0.831$) in the data base based on the fingerprint profile. AMF-26 was the only compound whose *r* value was higher than 0.8 of 4,000 compounds. As shown in Fig. 1*C*, the fingerprint of AMF-26 was similar to that of BFA, which suggested that AMF-26 has a similar biological mode of action to BFA. The mean logarithm of GI_{50} for AMF-26 was −7.33 (at 47 nM), which is comparable with that of BFA (−7.37 at 43 nM). These results indicated that AMF-26 possesses strong growth inhibitory activity as well as that of BFA.

Disassembly of the Golgi Apparatus Caused by AMF-26—COMPARE analysis indicated that AMF-26, like BFA, may be a Golgi disruptor. Therefore, we first examined whether AMF-26 induces Golgi disassembly by immunofluorescence staining with a monoclonal antibody to Golgi brefeldin A-resistant guanine nucleotide exchange factor 1 (GBF1). GBF1 is localized to the *cis*-Golgi apparatus and plays a role in vesicular trafficking by activating Arf1 (48). In control cells, GBF1 was observed in the perinuclear region, forming a ribbon-like structure (Fig. 2*A*). However, addition of BFA caused a rapid release of GBF1 into the cytoplasm (Fig. 2*B*). These results were in agreement with previously published reports (48). When the cells were treated with AMF-26, GBF1 was observed to be dispersed from the perinuclear region throughout the cytoplasm (Fig. 2*C*), which indicated that AMF-26 disrupted the Golgi apparatus. Moreover, this observation was confirmed by live imaging using the MDA-MB-435 stably expressing GFP-conjugated clathrin light chain a (CLCa) cells (supplemental Video S1, *A–C*). In MDA-MB-435/GFP-CLCa cells, the intensity of fluorescence signals of GFP-CLCa were periodically increased and decreased at the TGN, suggesting that the formation of clathrin-coated pits occurs synchronously and periodically at the TGN (23). Disruption of the Golgi apparatus was concurrent with the disappearance of GFP-CLCa signals suggesting that CLCa was affected by AMF-26. Next, we examined whether the

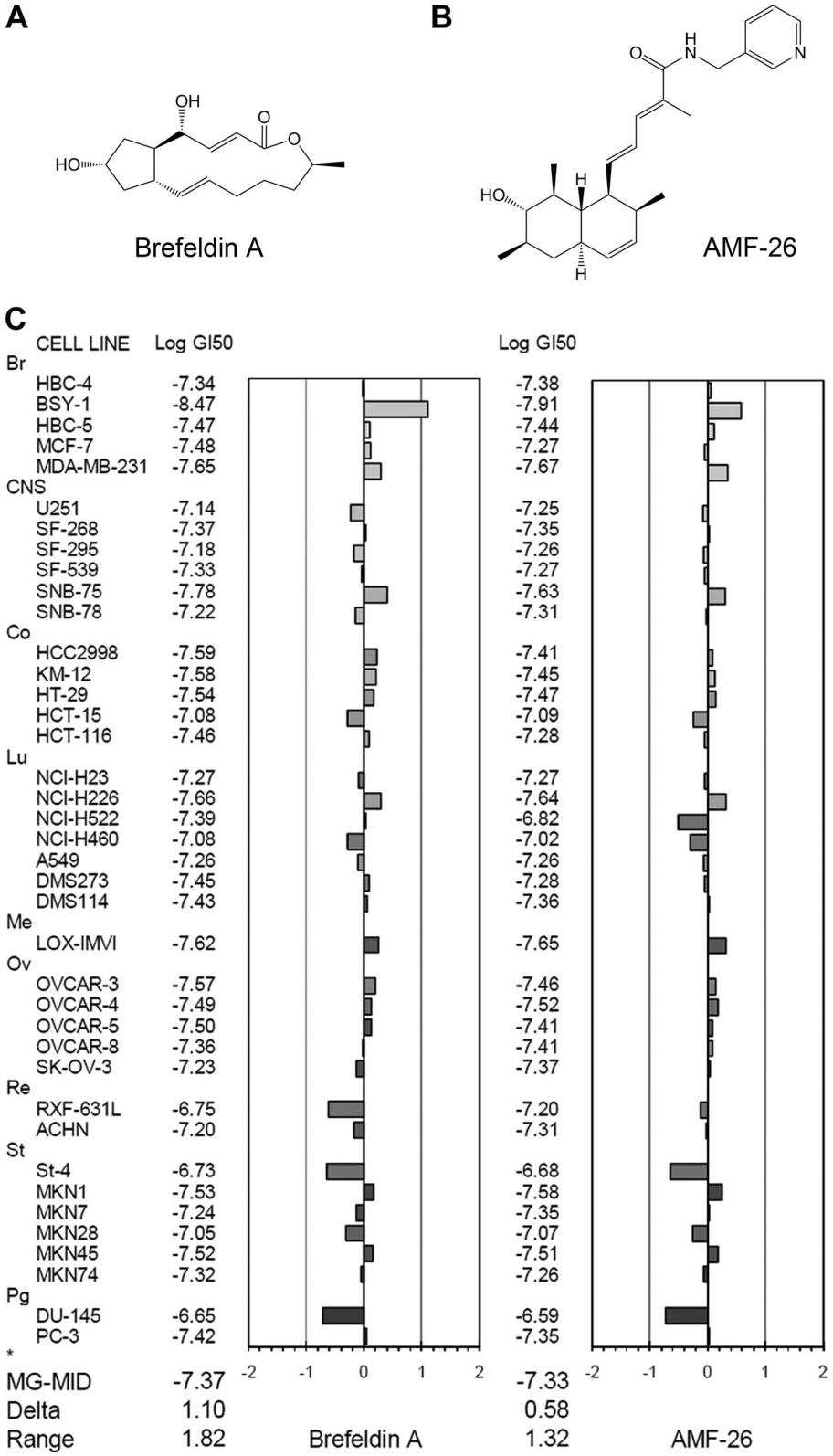

FIGURE 1. **Discovery of AMF-26 as a potent Golgi disruptor.** Chemical structure of (*A*) BFA and (*B*) AMF-26. *C*, growth inhibition against a panel of 39 human cancer cell lines. The mean graph was produced by computer processing of the 50% growth inhibition (GI_{50}) values as described under "Experimental Procedures." Logarithm of the GI_{50} value for each cell line is indicated. In the plot, columns to the *right* of zero indicate sensitivity of the cell line to the compound, and columns to the *left* indicate resistance to the compound. The *x* axis represents the logarithm of difference between the mean of GI_{50} values for 39 cell lines and the GI_{50} value for each cell line in the JFCR39 panel. The mean graph of AMF-26 (*right column*) is very similar to that of BFA (*left column*) (Pearson correlation coefficients; $r = 0.831$). MG-MID, the mean of log GI_{50} values for 39 cell lines; *Delta*, the logarithm of difference between the MG-MID and the log GI_{50} of the most sensitive cell line; *Range*, the logarithm of difference between the log GI_{50} of the most resistant cell line and the log GI_{50} of the most sensitive cell line. One scale represents one logarithm difference. Quantification of the GI_{50} value was represented as the mean of four different experiments. *Br*, breast; *CNS*, central nervous system; *Co*, colon; *Lu*, lung; *Me*, melanoma; *Ov*, ovarian; *Re*, renal; *St*, stomach; *xPg*, prostate.

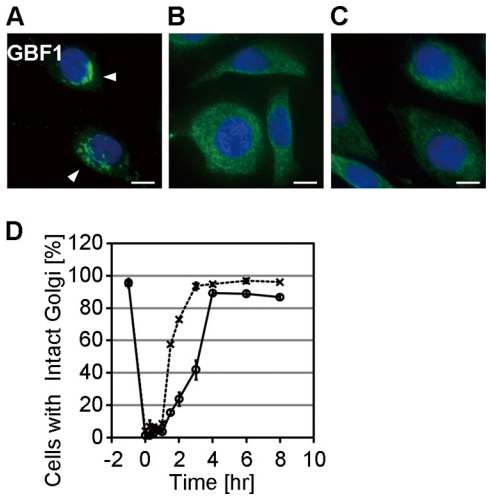

FIGURE 2. **AMF-26 disrupts Golgi apparatus in BSY-1 cells.** *A–C*, dispersion of Golgi in AMF-26-treated cells. BSY-1 cells were either untreated (*A*) or treated with (*B*) BFA (1 μM) or (*C*) AMF-26 (1 μM) for 1 h. Cells were fixed and labeled with anti-GBF1 (*green*) and DAPI (*blue*). GBF1 was dispersed from the perinuclear region, which gave a ribbon-like appearance (*white arrowhead*), into the cytoplasm of AMF-26- or BFA-treated cells. *Scale bar*, 20 μm. *D,* BSY-1 cells were treated with AMF-26 (1 μM) or BFA (1 μM) for 1 h, then washed with fresh medium and subsequently cultured without drugs for the indicated time. Thereafter, cells were fixed and stained with an antibody against GBF1. The images were analyzed by MetaMorph software. After the cells were cultured in medium without AMF-26 for 4 h, the normal Golgi structure reappeared in the perinuclear area. Symbols represent the following: *open circle*, AMF-26; *cross*, BFA. *Error bar*, S.D.

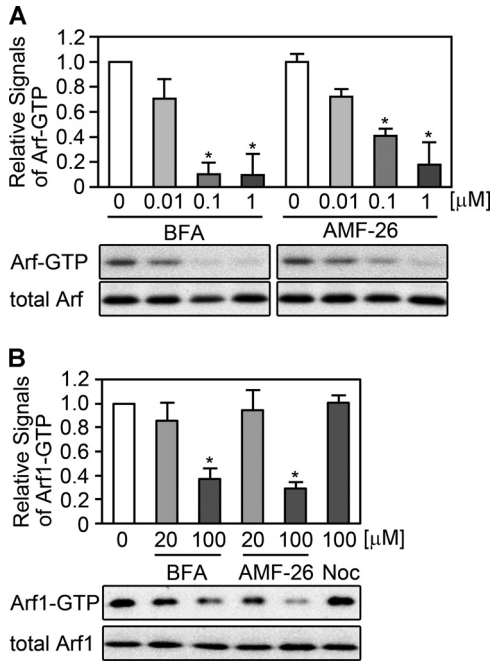

FIGURE 3. **AMF-26 causes the decrease in Arf1 activation.** *A*, BSY-1 cells were treated with DMSO, BFA, or AMF-26 at different concentrations for 1 h after 2 days preincubation. The cells were then lysed, and the extracts were incubated with immobilized GST-GGA3. Bound proteins were released and separated by SDS-PAGE and Western blotted. The signals of endogenous *pan*-Arfs-GTP was determined from the band intensity using ImageJ software. Treatment with AMF-26 or BFA for 1 h dramatically reduced the signals of endogenous *pan*-Arf-GTP in a dose-dependent manner. The relative signals of *pan*-Arf-GTP are represented as the mean of three different experiments. *B,* HEK293T cells transfected transiently with ARF1-HA for 24 h were exposed to DMSO, BFA, AMF-26, or nocodazole at the indicated concentrations for 1 h before lysis. The signals of exogenous Arf1-GTP were determined. Statistical analysis (Student's *t* test) was performed based on experiments done in triplicate. *Asterisks* represent statistically significant differences from untreated samples ($p < 0.05$). Abbreviations represent the following: *BFA*, brefeldin A; *Noc*, nocodazole. *Error bar*, S.D.

AMF-26-induced disruption of Golgi was a reversible process. The normal Golgi structure reappeared in the perinuclear area 4 h after washout of drugs with drug-free medium (Fig. 2*D*), which indicated that the effect of AMF-26 against Golgi was fully reversible like that of BFA (49).

Several tubulin polymerization inhibitors (*e.g.* nocodazole and vincristine) and ionophores (*e.g.* bafilomycin A1 and monensin) are known to disperse the Golgi apparatus (50, 51) as a consequence of disrupting microtubules (supplemental Fig. S1*C*) or intracellular pH (supplemental Fig. S1*F*). However, AMF-26 had no apparent effect on the structure of tubulin (supplemental Fig. S1*B*) or localization of lysosomes (supplemental Fig. S1*E*), suggesting that Golgi disruption induced by AMF-26 did not result from the disruption of microtubules or an alteration of intracellular pH.

Inhibition of Arf1 Activation by AMF-26 in Human Cells—By analogy to BFA, we reasoned that the disruption of Golgi via AMF-26 might be mediated through Arf1 inactivation. Then we measured the Arf activity in AMF-26-treated cells by an Arf-GTP pulldown assay that monitored the signals of Arf-GTP using the rGST-GGA3 protein (25, 26). The GAT domain of GGA3, an effector of Arf, preferentially binds the active Arf-GTP over the inactive Arf-GDP (25, 26). Treatment with AMF-26 or BFA for 1 h dramatically reduced the signals of endogenous *pan*-Arf-GTP in a dose-dependent manner within a range of submicromolar concentrations compared with the control state (Fig. 3*A*).

To further confirm that AMF-26 inhibited the activation of Arf1, we evaluated the signals of the exogenous Arf1 in HEK293T cells transiently transfected with human Arf1-HA. The signals of exogenous Arf1-GTP in the AMF-26 or BFA-treated cells for 1 h was significantly reduced in a dose-dependent manner compared with the control cells (Fig. 3*B*). At a concentration of 100 μM, AMF-26 and BFA reduced the signals of exogenous Arf1-GTP to 28.6 and 37.1%, respectively. These data suggested that AMF-26 caused Golgi disassembly by blocking Arf1 activation.

Comparison between the BFA and AMF-26 Complexes—To support this conclusion, we performed computer modeling/MD simulations. The octahydronaphthalene ring of AMF-26 (HP1, HP2, and DA1) was superimposed onto the lactone ring of BFA (HP1, HP2, and HA1) by SUPERPOSE (Fig. 4*C*). During the MD trajectory, the octahydronaphthalene ring of AMF-26 resided in the initial position. The refined model of the Arf1-AMF-26-Sec7 domain complex was compared with the X-ray structure of the Arf1-BFA-Sec7 domain complex (Fig. 4, *D* and *E*, supplemental Table S2). The same hydrophobic residues (Val-53, Thr-64, Trp-66, and Tyr-81 of Arf1 and Met-194, Thr-197, and Val-204 of Sec7 domain) interacted with the octahydronaphthalene ring of AMF-26 and the lactone ring of BFA. The hydrophobic interactions correspond to the matching of hydrophobic property spheres (HP1 and HP2) by SUPERPOSE. The positively charged Arg-19 of Arf1 interacted with the hydroxyl oxygen of AMF-26 and the carbonyl oxygen of BFA. This electrostatic interaction accounted for the match-

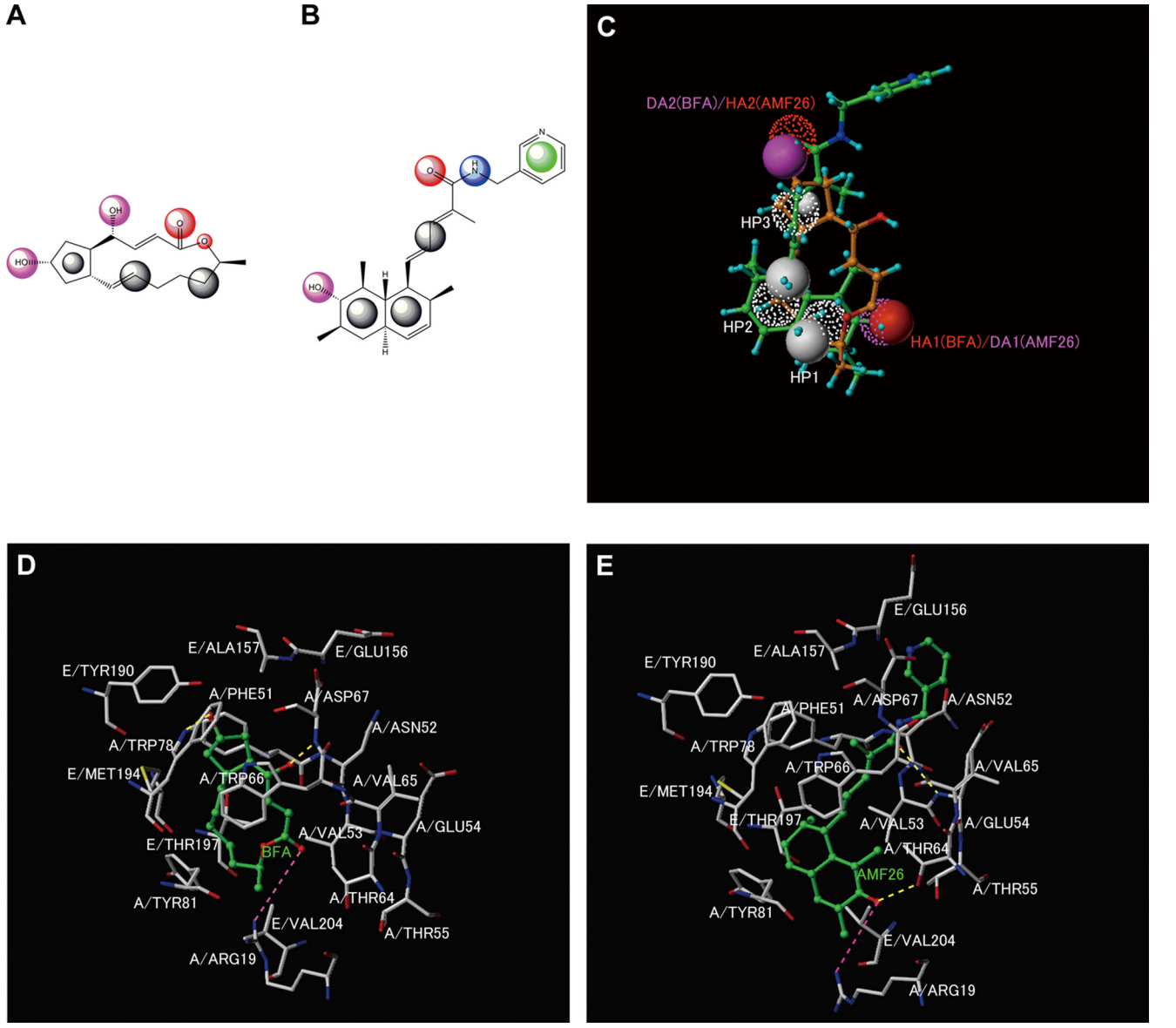

FIGURE 4. **Property spheres on BFA and AMF-26.** *A,* property spheres of BFA. *B,* property spheres of AMF-26. The *spheres* on each molecule are property spheres for molecular superposition. The colors of the spheres indicate the following properties: hydrophobic (HP; *black*), aromatic (AR; *green*), hydrogen-bond donors (HD; *blue*), hydrogen-bond acceptors (HA; *red*), and hydrogen-bond donors/acceptor (DA; *purple*). *Large* and *small spheres* indicate radii of 1 and 0.5 Å, respectively. *C*, superimposition of AMF-26 on BFA by the SUPERPOSE program. AMF-26 is shown in *green*, and BFA is shown in *orange*. Sphere colors indicate the following properties: hydrophobic (*white*), aromatic (*green*), hydrogen-bond donors (*blue*), hydrogen-bond acceptors (*red*), and hydrogen-bond donors/acceptor (*purple*). *Large* and *small spheres* represent radii of 1 and 0.5 Å, respectively. The AMF-26 and BFA spheres are represented by *dotted* and *solid spheres*, respectively. Only matched spheres are indicated. *D* and *E*, comparison between the BFA and AMF-26 complexes. *D,* X-ray structure of the Arf1-BFA-Sec7 domain complex (PDB ID 1r8q). *E,* refined model of the Arf1-AMF-26-Sec7 domain complex. *A* and *E* chains are Arf1 and Sec7 domain, respectively. The hydrogen bonds and the electrostatic interactions are indicated by *yellow* and *pink dashed lines*, respectively.

ing of hydrogen-bond acceptors (DA1 of AMF-26 and HA1 of BFA). In addition, the hydroxyl group of AMF-26 hydrogen-bonded to the side chain of Thr-64 of Arf1. Instead of the hydrogen bond between the hydroxyl oxygen of the lactone ring of BFA and the amide nitrogen of Asp-67 of Arf1, the amide oxygen of AMF-26 hydrogen-bonded with the main chain of Glu-54 of Arf1. This computer modeling/MD simulation suggested that AMF-26 bound to the contact surface of the Arf1-Sec7 domain where BFA is known to bind.

Effects of AMF-26 on the cis-Golgi, TGN, and Recycling Endosomes—To clarify the mechanism of Golgi disruption by AMF-26, we first examined the effect of AMF-26 on localization of *cis*-Golgi-associated proteins, βCOPI, GBF1, and p58/ERGIC53. COPI is the most important coat protein in facilitating retrograde intracellular transport from Golgi to the endoplasmic reticulum (ER) (52). In control cells, most of the βCOPI was localized on the *cis*-Golgi membrane, whereas the addition of AMF-26 caused a rapid release of βCOPI into the cytoplasm (Fig. 5*A*). GBF1, primarily localized in *cis*-Golgi as shown in Fig. 2, was dispersed into the cytoplasm of cells treated with AMF-26. Furthermore, treatment with AMF-26 caused the redistribution of p58/ERGIC53, a marker for the ER-Golgi intermediate compartment (*ERGIC)* (53), from its normal compact localization to a dispersed cytoplasmic

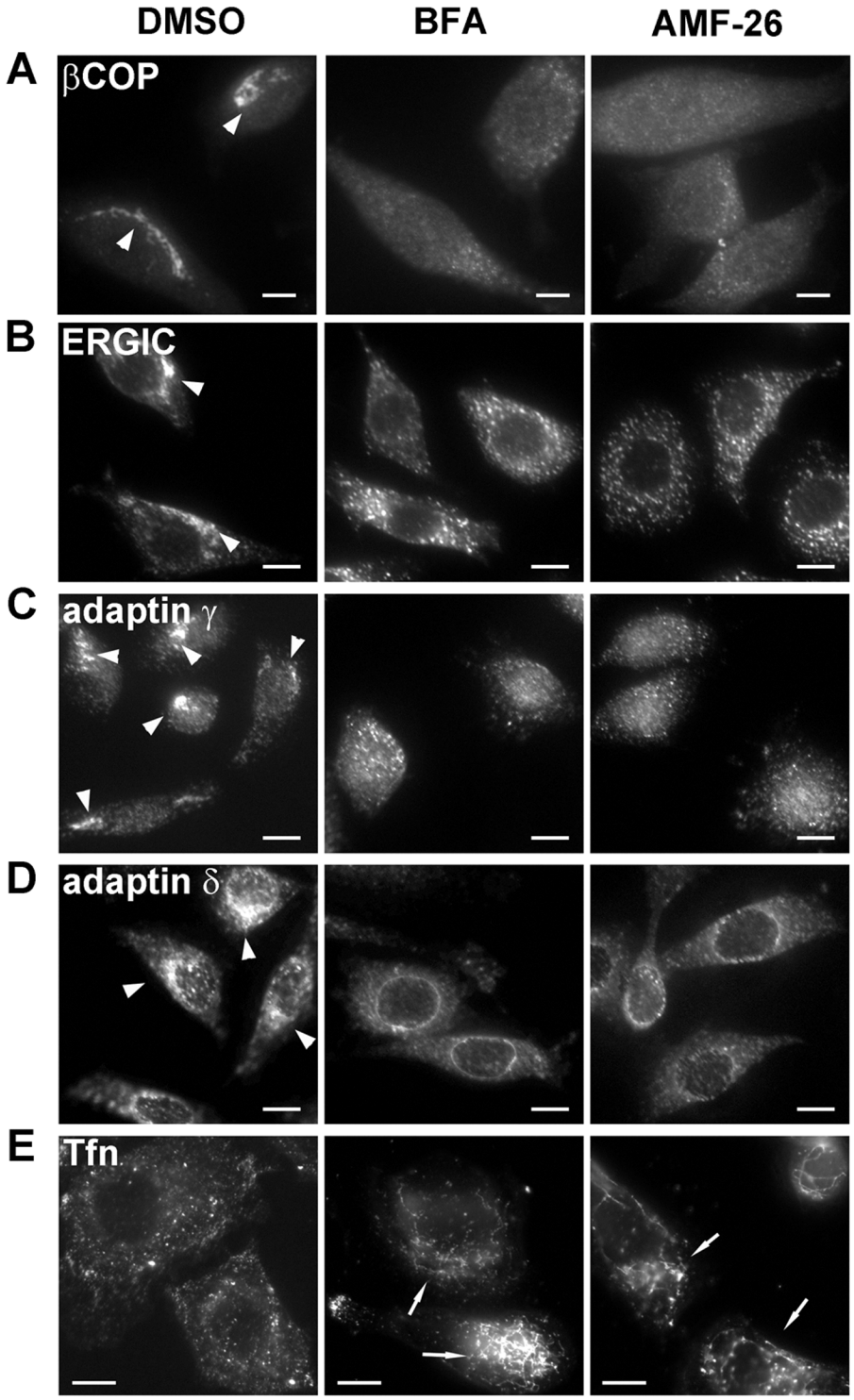

FIGURE 5. **Effects of AMF-26 on *cis*-Golgi, TGN, and recycling endosomes.** BSY-1 cells were incubated with DMSO, BFA (1 μM), or AMF-26 (1 μM) for 1 h. The labeling with each Golgi marker protein (*white*) was as follows: *A,* β-COP (*cis*-Golgi); *B,* ERGIC-53 (*cis*-Golgi and ERGIC); *C,* adaptin γ (TGN); or *D,* adaptin δ (TGN). The localization of *cis*-Golgi and TGN resulted in redistribution from the perinuclear region (*white arrowhead*) into the cytosol. *Scale bar*, 20 μm. *E,* BSY-1 cells were incubated with Alexa 488-labeled transferrin (*white*) for 1 h, and then treated with DMSO, BFA (1 μM), or AMF-26 (1 μM) for 1 h. AMF-26 induced extensive formation of membrane tubules from endosomes (*white arrow*). A similar result was found with BFA. *Scale bar*, 10 μm.

localization (Fig. 5*B*). These effects were similar to those of BFA.

We also examined the effects of AMF-26 on proteins associated with the TGN. AMF-26 affected adaptin γ or adaptin δ, constituents of AP-1 or AP-2, respectively (54), and eventually resulted in redistribution from the perinuclear region into the cytosol (Fig. 5, *C* and *D*).

Concerning recycling endosomes, treatment of BFA is known to induce extensive formation of membrane tubules from endosomes (10, 55). Using Alexa 488-labeled transferrin,

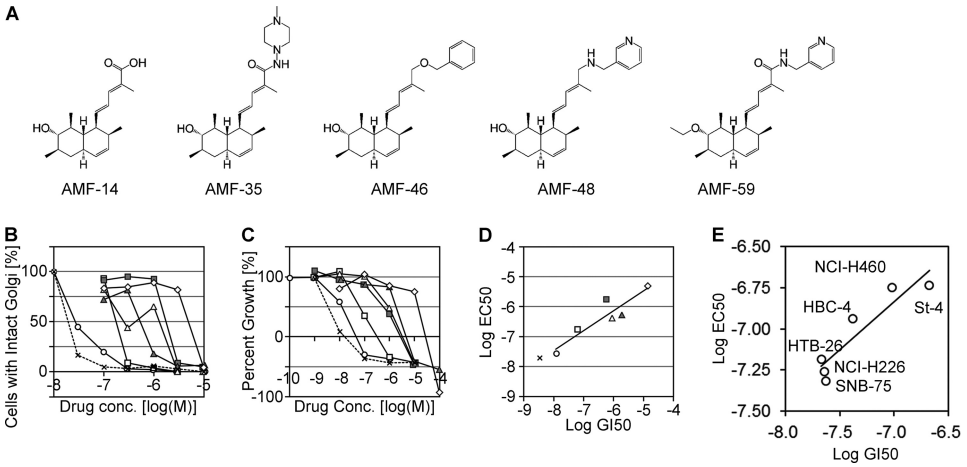

FIGURE 6. **Correlation between cell growth inhibition and Golgi disruption.** *A,* chemical structures of AMF-26 derivatives: AMF-14, AMF-35, AMF-46, AMF-48, and AMF-59. *B*, BSY-1 cells were treated with DMSO, AMF-26, and its derivatives, or BFA at different concentrations for 1 h, and then stained with antibodies against GBF-1. The numbers of cells whose Golgi was dispersed were then counted. Over 100 features were measured under each condition. *C*, the proliferation of BSY-1 cells treated with drugs was monitored as described above. Changes in the amounts of total cellular protein after 48 h of drug treatment were analyzed using the sulforhodamine B assay. *D,* Golgi dispersal activities were correlated with growth inhibitory activities between AMF-26 and its derivatives (Pearson correlation coefficients; $r = 0.92$, $p = 0.009$). Symbols represent the following: *open circle*, AMF-26; *open square*, AMF-48; *closed square*, AMF-59; *open triangle*, AMF-46; *closed triangle*, AMF-14; *open diamond*, AMF-35; cross, BFA-treated cells. *E*, Golgi dispersal activities were correlated with growth inhibitory activities between six cell lines of JFCR39 (Pearson correlation coefficients, $r = 0.93$, $p = 0.02$).

we analyzed the effect of AMF-26 on the formation of tubular endosomes. AMF-26 induced enlargement and tubulation of transferrin-positive endosomes (Fig. 5*E*), suggesting that AMF-26 has a similar effect on early/recycling endosomes as BFA.

Correlation between Cell Growth Inhibition and Golgi Disruption—It is still uncertain whether the growth-inhibitory activity of BFA is related to its effects on Golgi disruption (56, 57). We examined the correlation between cell growth inhibition and Golgi disruption activity to investigate the causal relationship of these two events. Specifically, we examined the activities of AMF-26 and its five derivatives AMF-14, AMF-35, AMF-46, AMF-48, and AMF-59 (structural formula of each compound shown in Fig. 6*A*). In BSY-1 cells, AMF-26 exhibited the strongest activity of cell growth inhibition with a GI_{50} of 12 nM and that of Golgi disruption with an EC_{50} of 27 nM. AMF-35 displayed the weakest activities with a GI_{50} and EC_{50} of 14 and 4.9 μM, respectively, (Fig. 6, *B* and *C*). We next investigated whether the Golgi disruption activities (the logarithm of EC_{50}) of these six compounds were related to their growth inhibitory activities (the logarithm of GI_{50}). Our analysis revealed a statistically significant correlation ($r = 0.92$ and $p = 0.009$) between these two activities (Fig. 6*D*). A statistically significant correlation between the logarithm of EC_{50} and the logarithm of GI_{50} was also observed when six other cell lines were treated with AMF-26 ($r = 0.93$ and $p = 0.02$, Fig. 6*E*). Taken together, our results suggested that there was a causal relationship between the Golgi disruption and cell growth inhibition.

AMF-26 Caused Apoptotic Cell Death—After a 24-h incubation with AMF-26, the sub-G_1 population increased in a dose-dependent manner over that of the DMSO-treated controls, *i.e.* 8.4 (AMF-26, 100 nM) *versus* 1.9% (Fig. 7*A*). These differences in the sub-G_1 population were even greater after 48 h, *i.e.* AMF-26-treated cells 13.1 (AMF-26, 100 nM) *versus* 2.1% (Fig. 7*A*). Furthermore, cleavage products of PARP were assessed by Western blot analysis of cell lysates (Fig. 7*B*). After incubation for 24 h, a band corresponding to cleaved PARP (89-kDa) was significantly stronger in cell extracts of AMF-26-treated cells compared with DMSO-treated cells. After 48 h, the larger accumulation of cleaved PARP in AMF-26-treated cells was obvious, suggesting apoptosis of AMF-26-treated cells.

Analysis of the Antitumor Efficacy of Orally Administrated AMF-26 Using Xenografts of Human Breast Cancer BSY-1—Finally, we evaluated the antitumor activity of AMF-26 against human breast cancer BSY-1 xenografts. After formation of the tumors (100–300 mm^3), mice were orally administered 0 (control vehicle), 83, or 100 mg/kg of AMF-26 for 5 consecutive days. Administration of AMF-26 at 83 or 100 mg/kg induced almost complete tumor regression on day 21 (Fig. 7*C, upper panel*). To assess toxicity, we measured the body weight of the tumor-bearing mice. The weight of the tumor-bearing mice was slightly reduced by administration of AMF-26. After termination of the administration, the weight was rapidly regained but was not fully recovered during the observation (Fig. 7*C, lower panel*). These data suggested that AMF-26 treatment did not cause serious irreversible side effects.

DISCUSSION

In this study, we identified a novel Golgi disruptor, AMF-26 using COMPARE analysis followed by computer modeling/MD simulation and biological validations. AMF-26 is thought to induce Golgi disruption via the inhibition of Arf1 activation. The Golgi disrupting activity of AMF-26 was significantly correlated with its growth-inhibiting activity. Finally, our results showed that oral administration of AMF-26 induced the regression of human breast cancer BSY-1 xenografts.

The Arf family of small GTPases plays a major role in maintaining Golgi structure and driving Golgi membrane traffic (5, 7). It is known that the BFA-sensitive large ArfGEFs, such as GBF1, BIG1, and BIG2, are predominantly localized to the *cis*-Golgi and TGN. After activation by GBF1, Arf1 mediates COPI

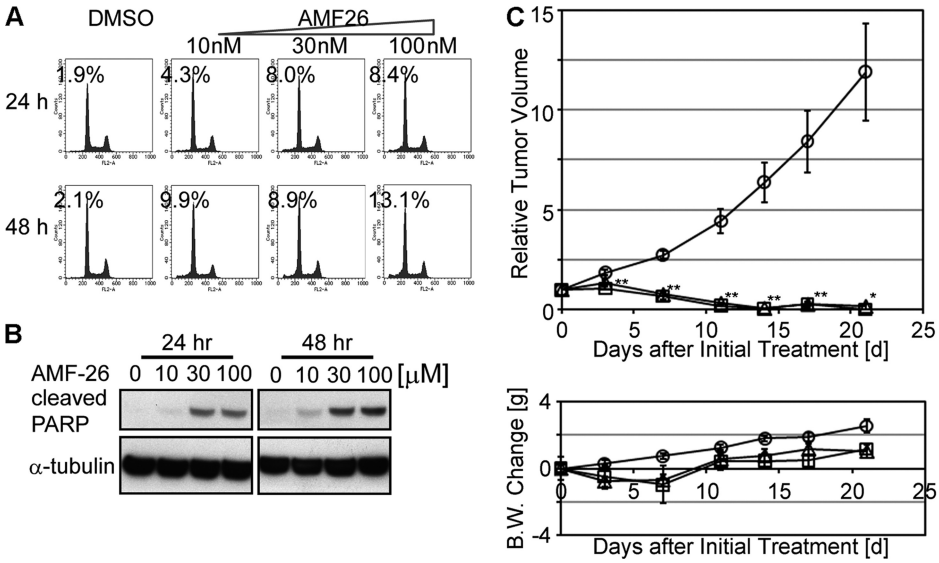

FIGURE 7. **Antitumor activity of AMF-26.** *A* and *B,* AMF-26 caused apoptosis on BSY-1 cell. *A,* cells were incubated with DMSO or with AMF-26 for 24 or 48 h. Percentages of the sub-G_1 population are indicated. AMF-26 influenced the sub-G_1 population in a dose-dependent manner. *B*, effect of AMF-26 on PARP cleavage. BSY-1 cells were incubated with AMF-26 for 24 or 48 h. Cells were lysed and the proteins in the cell extract were separated by SDS-PAGE and electroblotted onto a membrane. The membrane was then probed with antibodies against cleaved PARP and α-tubulin. Cleaved PARP protein was observed in AMF-26-treated cells. *C,* tumor growth and body weight in nude mice bearing human breast cancer BSY-1 xenografts. Fifteen nude mice were subcutaneously inoculated with a tumor fragment of 3 × 3 × 3 mm from the subcutaneous tumor developed in nude mice. When tumors reached a volume of 100–300 mm^3, animals were divided randomly into test groups, each with five mice (day 0). AMF-26 (83 or 100 mg/kg) was orally administered daily from day 0 to 5. AMF-26 data are the means of data from five mice. The *upper panel* shows the relative tumor volume. The *lower panel* shows the body weight change. Administration of AMF-26 induced complete tumor regression on day 21. *Asterisks* represent statistically significant differences from the control group (*, $p < 0.01$; **, $p < 0.005$). Symbols represent the following: *open circle*, control vehicle; *open square*, AMF-26 (83 mg/kg); *open triangle*, AMF-26 (100 mg/kg) was orally administrated group; *error bar*, S.E.

coat recruitment and enables vesicle transport between Golgi and ER (48). On the other hand, when activated by BIG1 or BIG2, Arf1 recruits adapter proteins, AP-1, AP-3, and AP-4(58), and Golgi-associated γ-adaptin ear-containing Arf-binding proteins, GGA1, GGA2, and GGA3 (59). These Arf1-effector molecules mediate transport between TGN and endosomes (58). BFA inactivates Arf1 by inhibiting PPIs between Arf1 and Arf1GEFs, and subsequently induces the disruption of *cis*-Golgi and TGN, or affects the endosomal systems (10, 11). Furthermore, BFA showed tumor growth inhibition *in vitro* (12) and *in vivo* at an early stage (13). From the viewpoint of developing molecular-targeted drugs, BFA is attractive because its target, Arf1 and ArfGEF interaction, is unique. However, BFA and its derivatives have not progressed beyond the preclinical stage of drug development (13, 14).

Here we used COMPARE analysis to screen for compounds showing a BFA-like fingerprint, and identified AMF-26. BFA has a lactone ring, whereas AMF-26 has an octahydronaphthalene ring with a side chain including a pyridine moiety. Although the chemical structure of AMF-26 is distinct from that of BFA, we verified that the two compounds share a similar molecular mode of action as expected from the COMPARE analysis. Moreover, computer modeling/MD simulation and biological validations suggested that AMF-26 inhibited the interaction between Arf1 and BFA-sensitive large ArfGEFs. AMF-26 induced the disruption of *cis*-Golgi and TGN at almost the same concentrations as BFA, and inhibited recycling of transferrin. These results indicate that AMF-26 is a novel inhibitor of Arf1 activation whose chemical structure is different from BFA.

Several other Golgi disruptors related to Arf activation have been reported (44, 57, 60–62). These compounds showed inhibition of membrane traffic. However, their precise modes of action appear to be different from that of AMF-26 and BFA. Moreover, compared with AMF-26 or BFA, these compounds resulted in much weaker inhibition of cell growth.

It remains uncertain whether cell growth inhibition by BFA arises from Golgi disruption. Citterio *et al.* (56) indicated that decreased expression of GBF1, BIG1, or BIG2 by siRNA caused dispersion of the Golgi-localized protein and the inhibition of cell growth. We observed similar results in BSY-1 cells in our preliminary data.[3] However, Pan *et al.* (57) reported that AG1478 showed a weak loss of cell viability. In the present study, we demonstrated that AMF-26 inhibited both Arf1 activation and tumor cell growth in BSY-1 cells. Moreover, AMF-26 and its derivatives showed a positive correlation between the Golgi-disrupting activity and the cell growth-inhibiting activity. We also found a positive correlation between the two when six other cancer cell lines were treated with AMF-26. In our preliminary experiments, inactivation of the phosphatidylinositol 3-kinase pathway or Ras-MAPK pathway was not observed by exposure of cells to AMF-26 for 10 min (data not shown). Collectively, our results suggested a causal relationship between Golgi disruption and cell growth inhibition by AMF-26. Furthermore, in the present study, we found that AMF-26 induced apoptosis in tumor cells. Our observations agree with the report of Citterio *et al.* (56) indicating that decreased expression of GBF1 causes apoptosis.

A previous study described the antitumor activity of BFA in early stage mouse subcutaneous models (13). In the course of

[3] Y. Ohashi, H. Iijima, N. Yamaotsu, K. Yamazaki, S. Sato, M. Okamura, K. Sugimoto, S. Dan, and T. Yamori, unpublished data.

these studies, BFA was injected intraperitoneally twice a day. Frequent administration was necessary because the clearance of BFA is rapid (less than 20 min) (13), consistent with the observation that this compound is a substrate of glutathione *S*-transferase (63). Here, we demonstrated that oral administration of AMF-26 once a day induced almost complete regression of human breast cancer BSY-1 xenografts in nude mice. To the best of our knowledge, this is the first report describing the oral administration of an inhibitor targeting Arf1 activation that elicits strong antitumor activity without severe body weight loss. Further study on the pharmacokinetic profile of AMF-26 remains to be performed.

Very recently, AMF-26 was identified as an angiogenesis inhibitor by Watari *et al.* (64), who revealed that inhibition of VEGF receptor phosphorylation and NF-κB signaling was involved in antiangiogenic activity in human umbilical vein endothelial cells. Therefore, the *in vivo* antitumor activity of AMF-26 shown in the present study may have partly resulted from its antiangiogenic activity in addition to its direct tumor growth inhibition.

The COMPARE analysis is a powerful tool that can be used to identify small-molecule enzyme inhibitors, for example, telomerase inhibitor (FJ-5002) (45), a topoisomerase I and II inhibitor (MS-247) (19), and PI3K inhibitor (ZSTK474) (22, 46, 47). In this study, we exploited the COMPARE analysis to screen BFA-like small molecule inhibitors. Using this approach, we identified AMF-26 as a novel inhibitor of Arf1 activation, despite the fact that its chemical structure does not resemble that of BFA. From these results, the screening of chemicals guided by COMPARE analysis appears to be useful for the discovery of novel drug candidates targeting various biological functions including the Golgi system.

In conclusion, we identified a novel Golgi disruptor targeting Arf1 activation, AMF-26, and showed that it induced complete regression of human breast cancer BSY-1 xenografts. These data suggest that AMF-26 is a novel drug candidate for cancer treatment targeting Arf1 activation.

Acknowledgments—We thank Dr. R. H. Shoemaker and Dr. K. D. Paull for discussion on the establishment of JFCR39 and COMPARE analysis; Y. Nishimura, M. Seki, Y. Mukai, and Y. Yamazaki for technical assistance; NIPPON SHINYAKU CO., Ltd. for provision of AMF-26 and its derivatives and for discussion concerning the nature of the compounds; and Dr. S Sakaushi (Osaka Prefecture University, Osaka, Japan) for advice on time lapse analysis.

REFERENCES

1. Berg, T. (2008) Small-molecule inhibitors of protein-protein interactions. *Curr. Opin. Drug Discov. Devel.* **11,** 666–674
2. Wells, J. A., and McClendon, C. L. (2007) Reaching for high-hanging fruit in drug discovery at protein-protein interfaces. *Nature* **450,** 1001–1009
3. Lauria, A., Tutone, M., Ippolito, M., Pantano, L., and Almerico, A. M. (2010) Molecular modeling approaches in the discovery of new drugs for anti-cancer therapy. The investigation of p53-MDM2 interaction and its inhibition by small molecules. *Curr. Med. Chem.* **17,** 3142–3154
4. Azmi, A. S., and Mohammad, R. M. (2009) Non-peptidic small molecule inhibitors against Bcl-2 for cancer therapy. *J. Cell Physiol.* **218,** 13–21
5. D'Souza-Schorey, C., and Chavrier, P. (2006) ARF proteins. Roles in membrane traffic and beyond. *Nat. Rev. Mol. Cell Biol.* **7,** 347–358
6. Mossessova, E., Gulbis, J. M., and Goldberg, J. (1998) Structure of the guanine nucleotide exchange factor Sec7 domain of human arno and analysis of the interaction with ARF GTPase. *Cell* **92,** 415–423
7. Casanova, J. E. (2007) Regulation of Arf activation. The Sec7 family of guanine nucleotide exchange factors. *Traffic* **8,** 1476–1485
8. Renault, L., Guibert, B., and Cherfils, J. (2003) Structural snapshots of the mechanism and inhibition of a guanine nucleotide exchange factor. *Nature* **426,** 525–530
9. Zeeh, J. C., Zeghouf, M., Grauffel, C., Guibert, B., Martin, E., Dejaegere, A., and Cherfils, J. (2006) Dual specificity of the interfacial inhibitor brefeldin A for ARF proteins and Sec7 domains. *J. Biol. Chem.* **281,** 11805–11814
10. Lippincott-Schwartz, J., Yuan, L., Tipper, C., Amherdt, M., Orci, L., and Klausner, R. D. (1991) Brefeldin A effects on endosomes, lysosomes, and the TGN suggest a general mechanism for regulating organelle structure and membrane traffic. *Cell* **67,** 601–616
11. Lippincott-Schwartz, J., Yuan, L. C., Bonifacino, J. S., and Klausner, R. D. (1989) Rapid redistribution of Golgi proteins into the ER in cells treated with brefeldin A. Evidence for membrane cycling from Golgi to ER. *Cell* **56,** 801–813
12. Häcki, J., Egger, L., Monney, L., Conus, S., Rossé, T., Fellay, I., and Borner, C. (2000) Apoptotic cross-talk between the endoplasmic reticulum and mitochondria controlled by Bcl-2. *Oncogene* **19,** 2286–2295
13. Sausville, E. A., Duncan, K. L., Senderowicz, A., Plowman, J., Randazzo, P. A., Kahn, R., Malspeis, L., and Grever, M. R. (1996) Antiproliferative effect *in vitro* and antitumor activity *in vivo* of brefeldin A. *Cancer J. Sci. Am.* **2,** 52–58
14. Anadu, N. O., Davisson, V. J., and Cushman, M. (2006) Synthesis and anticancer activity of brefeldin A ester derivatives. *J. Med. Chem.* **49,** 3897–3905
15. Monks, A., Scudiero, D., Skehan, P., Shoemaker, R., Paull, K., Vistica, D., Hose, C., Langley, J., Cronise, P., and Vaigro-Wolff, A. (1991) Feasibility of a high-flux anticancer drug screen using a diverse panel of cultured human tumor cell lines. *J. Natl. Cancer Inst.* **83,** 757–766
16. Paull, K. D., Shoemaker, R. H., Hodes, L., Monks, A., Scudiero, D. A., Rubinstein, L., Plowman, J., and Boyd, M. R. (1989) Display and analysis of patterns of differential activity of drugs against human tumor cell lines. Development of mean graph and COMPARE algorithm. *J. Natl. Cancer Inst.* **81,** 1088–1092
17. Shoemaker, R. H. (2006) The NCI60 human tumor cell line anticancer drug screen. *Nat. Rev. Cancer* **6,** 813–823
18. Yamori, T. (2003) Panel of human cancer cell lines provides valuable database for drug discovery and bioinformatics. *Cancer Chemother. Pharmacol.* **52,** Suppl. 1, S74–79
19. Yamori, T., Matsunaga, A., Sato, S., Yamazaki, K., Komi, A., Ishizu, K., Mita, I., Edatsugi, H., Matsuba, Y., Takezawa, K., Nakanishi, O., Kohno, H., Nakajima, Y., Komatsu, H., Andoh, T., and Tsuruo, T. (1999) Potent antitumor activity of MS-247, a novel DNA minor groove binder, evaluated by an *in vitro* and *in vivo* human cancer cell line panel. *Cancer Res.* **59,** 4042–4049
20. Dan, S., Tsunoda, T., Kitahara, O., Yanagawa, R., Zembutsu, H., Katagiri, T., Yamazaki, K., Nakamura, Y., and Yamori, T. (2002) An integrated database of chemosensitivity to 55 anticancer drugs and gene expression profiles of 39 human cancer cell lines. *Cancer Res.* **62,** 1139–1147
21. Sharma, S. V., Haber, D. A., and Settleman, J. (2010) Cell line-based platforms to evaluate the therapeutic efficacy of candidate anticancer agents. *Nat. Rev. Cancer* **10,** 241–253
22. Yaguchi, S., Fukui, Y., Koshimizu, I., Yoshimi, H., Matsuno, T., Gouda, H., Hirono, S., Yamazaki, K., and Yamori, T. (2006) Antitumor activity of ZSTK474, a new phosphatidylinositol 3-kinase inhibitor. *J. Natl. Cancer Inst.* **98,** 545–556
23. Sakaushi, S., Senda-Murata, K., Fukada, T., Oka, S., and Sugimoto, K. (2007) Rhythmic cycle of clathrin-coated pit formation at the *trans*-Golgi network in human MDA-MB-435 cells. *Biosci. Biotechnol. Biochem.* **71,** 571–574
24. Skehan, P., Storeng, R., Scudiero, D., Monks, A., McMahon, J., Vistica, D., Warren, J. T., Bokesch, H., Kenney, S., and Boyd, M. R. (1990) New colorimetric cytotoxicity assay for anticancer drug screening. *J. Natl. Cancer Inst.* **82,** 1107–1112

25. Takatsu, H., Yoshino, K., Toda, K., and Nakayama, K. (2002) GGA proteins associate with Golgi membranes through interaction between their GGAH domains and ADP-ribosylation factors. *Biochem. J.* **365,** 369–378
26. Puertollano, R., Randazzo, P. A., Presley, J. F., Hartnell, L. M., and Bonifacino, J. S. (2001) The GGAs promote ARF-dependent recruitment of clathrin to the TGN. *Cell* **105,** 93–102
27. Tsujishita, H., and Hirono, S. (1997) CAMDAS, an automated conformational analysis system using molecular dynamics. Conformational analyzer with molecular dynamics and sampling. *J. Comput. Aided Mol. Des.* **11,** 305–315
28. Halgren, T. A. (1999) MMFF VI. MMFF94s option for energy minimization studies. *J. Comput. Chem.* **20,** 720–729
29. Halgren, T. A. (1999) MMFF VII. Characterization of MMFF94, MMFF94s, and other widely available force fields for conformational energies and for intermolecular-interaction energies and geometries. *J. Comput. Chem.* **20,** 730–748
30. Iwase, K., and Hirono, S. (1999) Estimation of active conformations of drugs by a new molecular superposing procedure. *J. Comput. Aided Mol. Des.* **13,** 499–512
31. Cornell, W. D., Cieplak, P., Bayly, C. I., Gould, I. R., Merz, K. M., Jr., Ferguson, D. M., Spellmeyer, D. C., Fox, T., Caldwell, J. W., and Kollman, P. A. (1995) A second generation force field for the simulation of proteins, nucleic acids, and organic molecules. *J. Am. Chem. Soc.* **117,** 5179–5197
32. Gasteiger, J., and Marsili, M. (1980) Iterative partial equalization of orbital electronegativity—a rapid access to atomic charges. *Tetrahedron* **36,** 3219–3228
33. Gasteiger, J., and Marsili, M. (1981) Prediction of proton magnetic resonance shifts: the dependence on hydrogen charges obtained by iterative partial equalization of orbital electronegativity. *Organ. Magn. Reson.* **15,** 353–360
34. Marsili, M., and Gasteiger, J. (1980) Pi-charge distributions from molecular topology and pi-orbital electronegativity. *Croat. Chem. Acta* **53,** 601–614
35. Purcel, W. P., and Singer, J. A. (1967) A brief review and table of semiempirical parameters used in the Hueckel molecular orbital method. *J. Chem. Eng. Data* **12,** 235–246
36. Case, D. A., Darden, T. A., Cheatham, T. E., III, Simmerling, C. L., Wang, J., Duke, R. E., Luo, R., Merz, K. M., Pearlman, D. A., Crowley, M., Walker, R. C., Zhang, W., Wang, B., Hayik, S., Roitberg, A., Seabra, G., Wong, K. F., Paesani, F., Wu, X., Brozell, S., Tsui, V., Gohlke, H., Yang, L., Tan, C., Mongan, J., Hornak, V., Cui, G., Beroza, P., Mathews, D. H., Schafmeister, C., Ross, W. S., and Kollman, P. A. (2006) *AMBER* 9, University of California, San Francisco, CA
37. Wang, J., Cieplak, P., and Kollman, P. A. (2000) How well does a restrained electrostatic potential (RESP) model perform in calculating conformational energies of organic and biological molecules? *J. Comput. Chem.* **21,** 1049–1074
38. Wang, J., Wolf, R. M., Caldwell, J. W., Kollman, P. A., and Case, D. A. (2004) Development and testing of a general Amber force field. *J. Comput. Chem.* **25,** 1157–1174
39. Cieplak, P., Cornel, W. D., Bayly, C., and Kollman, P. A. (1995) Application of the multimolecule and multiconformational RESP methodology to biopolymers: Charge derivation for DNA, RNA, and proteins. *J. Comput. Chem.* **16,** 1357–1377
40. Frisch, M. J., Trucks, G. W., Schlegel, H. B., Scuseria, G. E., Robb, M. A., Cheeseman, J. R., Montgomery, Jr., J. A., Vreven, T., Kudin, K. N., Burant, J. C., Millam, J. M., Iyengar, S. S. T. J., Barone, V., Mennucci, B., Cossi, M., Scalmani, G., Rega, N., Petersson, G. A., Nakatsuji, H., Hada, M., Ehara, M., Toyota, K., Fukuda, R., Hasegawa, J., Ishida, M., Nakajima, T., Honda, Y., Kitao, O., Nakai, H., Klene, M., Li, X., Knox, J. E., Hratchian, H. P., Cross, J. B., Bakken, V., Adamo, C., Jaramillo, J., Gomperts, R., Stratmann, R. E., Yazyev, O., Austin, A. J., Cammi, R., Pomelli, C., Ochterski, J. W., Ayala, P. Y., Morokuma, K., Voth, G. A., Salvador, P., Dannenberg, J. J., Zakrzewski, V. G., Dapprich, S., Daniels, A. D., Strain, M. C., Farkas, O., Malick, D. K., Rabuck, A. D., Raghavachari, K., Foresman, J. B., Ortiz, J. V., Cui, Q., Baboul, A. G., Clifford, S., Cioslowski, J., Stefanov, B. B., Liu, G., Liashenko, A., Piskorz, P., Komaromi, I., Martin, R. L., Fox, D. J., Keith, T., Al-Laham, M. A., Peng, C. Y., Nanayakkara, A., Challacombe, M., Gill, P. M., Johnson, B., Chen, W., Wong, M. W., Gonzalez, C., and Pople, J. A. (2004) *Gaussian 03, Revision C.02*, Gaussian, Inc., Wallingford, CT
41. Jorgensen, W. L., Chandrasekhar, J., Madura, J., and Klein, M. L. (1983) Comparison of simple potential functions for simulating liquid water. *J. Chem. Phys.* **79,** 926–935
42. Darden, T., York, D., and Pedersen, L. (1993) Particle mesh Ewald: An N·log(N) method for Ewald sums in large systems. *J. Chem. Phys.* **98,** 10089–10092
43. Ryckaert, J. P., Ciccotti, G., and Berendsen, H. J. (1977) Numerical integration of the cartesian equations of motion of a system with constraints: molecular dynamics of n-alkanes. *J. Comput. Phys.* **23,** 327–341
44. Sáenz, J. B., Sun, W. J., Chang, J. W., Li, J., Bursulaya, B., Gray, N. S., and Haslam, D. B. (2009) Golgicide A reveals essential roles for GBF1 in Golgi assembly and function. *Nat. Chem. Biol.* **5,** 157–165
45. Naasani, I., Seimiya, H., Yamori, T., and Tsuruo, T. (1999) FJ5002, a potent telomerase inhibitor identified by exploiting the disease-oriented screening program with COMPARE analysis. *Cancer Res.* **59,** 4004–4011
46. Dan, S., Okamura, M., Seki, M., Yamazaki, K., Sugita, H., Okui, M., Mukai, Y., Nishimura, H., Asaka, R., Nomura, K., Ishikawa, Y., and Yamori, T. (2010) Correlating phosphatidylinositol 3-kinase inhibitor efficacy with signaling pathway status. *In silico* and biological evaluations. *Cancer Res.* **70,** 4982–4994
47. Kong, D., Dan, S., Yamazaki, K., and Yamori, T. (2010) Inhibition profiles of phosphatidylinositol 3-kinase inhibitors against PI3K superfamily and human cancer cell line panel JFCR39. *Eur. J. Cancer* **46,** 1111–1121
48. Niu, T. K., Pfeifer, A. C., Lippincott-Schwartz, J., and Jackson, C. L. (2005) Dynamics of GBF1. A brefeldin A-sensitive Arf1 exchange factor at the Golgi. *Mol. Biol. Cell* **16,** 1213–1222
49. Thyberg, J., and Moskalewski, S. (1999) Role of microtubules in the organization of the Golgi complex. *Exp. Cell Res.* **246,** 263–279
50. Morré, D. J., Minnifield, N., and Mollenhauer, H. H. (1985) Kinetics of monensin-induced swelling of Golgi apparatus cisternae of H-2 hepatoma cells. *Eur. J. Cell Biol.* **37,** 107–110
51. Thyberg, J., and Moskalewski, S. (1989) Subpopulations of microtubules with differential sensitivity to nocodazole. Role in the structural organization of the Golgi complex and the lysosomal system. *J. Submicrosc. Cytol. Pathol.* **21,** 259–274
52. Presley, J. F., Ward, T. H., Pfeifer, A. C., Siggia, E. D., Phair, R. D., and Lippincott-Schwartz, J. (2002) Dissection of COPI and Arf1 dynamics *in vivo* and role in Golgi membrane transport. *Nature* **417,** 187–193
53. Appenzeller-Herzog, C., and Hauri, H. P. (2006) The ER-Golgi intermediate compartment (ERGIC). In search of its identity and function. *J. Cell Sci.* **119,** 2173–2183
54. Nakayama, K., and Wakatsuki, S. (2003) The structure and function of GGAs, the traffic controllers at the TGN sorting cross-roads. *Cell Struct. Funct.* **28,** 431–442
55. Wood, S. A., Park, J. E., and Brown, W. J. (1991) Brefeldin A causes a microtubule-mediated fusion of the *trans*-Golgi network and early endosomes. *Cell* **67,** 591–600
56. Citterio, C., Vichi, A., Pacheco-Rodriguez, G., Aponte, A. M., Moss, J., and Vaughan, M. (2008) Unfolded protein response and cell death after depletion of brefeldin A-inhibited guanine nucleotide-exchange protein GBF1. *Proc. Natl. Acad. Sci. U.S.A.* **105,** 2877–2882
57. Pan, H., Yu, J., Zhang, L., Carpenter, A., Zhu, H., Li, L., Ma, D., and Yuan, J. (2008) A novel small molecule regulator of guanine nucleotide exchange activity of the ADP-ribosylation factor and Golgi membrane trafficking. *J. Biol. Chem.* **283,** 31087–31096
58. Ishizaki, R., Shin, H. W., Mitsuhashi, H., and Nakayama, K. (2008) Redundant roles of BIG2 and BIG1, guanine-nucleotide exchange factors for ADP-ribosylation factors in membrane traffic between the *trans*-Golgi network and endosomes. *Mol. Biol. Cell* **19,** 2650–2660
59. Doray, B., Ghosh, P., Griffith, J., Geuze, H. J., and Kornfeld, S. (2002) Cooperation of GGAs and AP-1 in packaging MPRs at the *trans*-Golgi network. *Science* **297,** 1700–1703
60. Viaud, J., Zeghouf, M., Barelli, H., Zeeh, J. C., Padilla, A., Guibert, B., Chardin, P., Royer, C. A., Cherfils, J., and Chavanieu, A. (2007) Structure-based discovery of an inhibitor of Arf activation by Sec7 domains through targeting of protein-protein complexes. *Proc. Natl. Acad. Sci. U.S.A.* **104,**

10370–10375
61. Feng, Y., Yu, S., Lasell, T. K., Jadhav, A. P., Macia, E., Chardin, P., Melancon, P., Roth, M., Mitchison, T., and Kirchhausen, T. (2003) Exo1, a new chemical inhibitor of the exocytic pathway. *Proc. Natl. Acad. Sci. U.S.A.* **100,** 6469–6474
62. Feng, Y., Jadhav, A. P., Rodighiero, C., Fujinaga, Y., Kirchhausen, T., and Lencer, W. I. (2004) Retrograde transport of cholera toxin from the plasma membrane to the endoplasmic reticulum requires the *trans*-Golgi network but not the Golgi apparatus in Exo2-treated cells. *EMBO Rep.* **5,** 596–601
63. Brüning, A., Ishikawa, T., Kneusel, R. E., Matern, U., Lottspeich, F., and Wieland, F. T. (1992) Brefeldin A binds to glutathione *S*-transferase and is secreted as glutathione and cysteine conjugates by Chinese hamster ovary cells. *J. Biol. Chem.* **267,** 7726–7732
64. Watari, K., Nakamura, M., Fukunaga, Y., Furuno, A., Shibata, T., Kawahara, A., Hosoi, F., Kuwano, T., Kuwano, M., and Ono, M. (2011) The antitumor effect of a novel angiogenesis inhibitor (an octahydronaphthalene derivative) targeting both VEGF receptor and NF-κB pathway. *Int. J. Cancer* doi: 10.1002/ijc.26356